RSC Advances

ROYAL SOCIETY OF CHEMISTRY

www.rsc.org/advances

RSC Advances

PAPER

Simultaneous reduction and nitrogen doping of graphite oxide by using electron beam irradiation

Received 00th January 20xx,
Accepted 00th January 20xx

DOI: 10.1039/x0xx00000x

www.rsc.org/

M. Kang,[a] D. H. Lee,[a] J. Yang,[b] Y.-M. Kang,[b] and H. Jung,*[a]

Nitrogen-doped graphenes (NGs) were successfully obtained by electron beam (e-beam) irradiation from graphite oxide (GO) colloid solution in the presence of aqueous ammonia at room temperature under ambient condition. The morphology, structure, and components of the obtained NGs were characterized by scanning electron microscopy, Raman spectroscopy, powder X-ray diffraction, elemental analysis, and X-ray photoelectron spectroscopy. The amount of incorporated nitrogen was in the range ~3.20 – 3.54 wt% with pyrrolic-N as the main nitrogen configuration. The results of this study show that nitrogen was simultaneously doped into graphene as the GO was reduced by e-beam irradiation. Herein, the ratio of nitrogen sites (pyridinic-N, pyrrolic-N, graphitic-N, and pyridinic-N-oxide) and specific surface area were controlled for various applications of the NGs as a function of irradiation dose. Increasing concentrations of graphitic-N and pyridinic-N-oxide enhanced the electrical conductivity and improved the kinetic performance of supercapacitor. The highest capacitance of 90.5 F g^{-1} at a charge/discharge current of 0.1 A g^{-1} in organic media was achieved for NG-300 because of a high BET specific surface area of 470 m^2 g^{-1}.

Introduction

Graphene, a single-atom-thick sheet of sp^2-hybridized carbon with honeycomb structure, has attracted tremendous interest as a key material in various fields such as electronic devices,[1] sensors,[2] photocatalysts,[3] energy storage materials,[4,5] and polymer nanocomposites,[6] owing to its unique physical, chemical, and mechanical properties.[7-9] However, these properties of graphene still lack of fulfilling the demand of various applications because of its low intrinsic capacitance and zero bandgap.[7,10] Recently, significant efforts have been reported introducing hetero-ion into graphene lattice for modulating and improving its intrinsic properties such as band structure, electronic properties, and surface chemistry for various applications.[11-17] Among the numerous potential dopants, nitrogen is considered to be an excellent candidate for the doping into graphene, because of its similar atomic size and five valence electrons available to form aromatic bonds with carbon atoms.[18]

Until now, nitrogen-doped graphenes (NGs) have been synthesized by various fabrication methods such as nitrogen plasma process,[19] chemical vapor deposition (CVD) of methane in the presence of ammonia,[20] thermal annealing of graphite oxide (GO) under flowing ammonia,[21] hydrothermal, solvothermal, or microwave-assisted reduction of GO with nitrogen source such as urea and ammonia water.[5,11,22] However, the realization of these applications is still not practical, because of the limitations for large-scale and safe production of NGs. Recently, the reduction of GO has been achieved through the radiolysis method. In comparison with the conventional approach, this strategy has many advantages such as chemical reductant free, cost-effective, eco-friendly, and easily scaled-up.[23-26] In this regard, e-beam irradiation can be adapted to reduce GO and simultaneously doping nitrogen into the carbon network, even at room temperature under ambient air conditions. To the best of our knowledge, one-pot approach for the synthesis of NGs by using e-beam irradiation has not yet been reported. In this study, we systematically investigated the effect of e-beam irradiation dose on the physicochemical properties such as pore structure, specific surface area (SSA), conductivity, nitrogen configuration as well as electrochemical performances of the NGs. In particular, nitrogen configuration and SSA of NGs is quite important for controlling various properties such as surface charge, doping type, and interface for various applications.

In this work, we present a simple one-pot approach to obtain NGs by using e-beam irradiation (Scheme 1). Because ammonia tends to react with the carboxylic acid functional groups of GO to form intermediate, aqueous ammonia was introduced as the nitrogen source.[27] And then, the intermediate can be reduced by the hydrated electron, which was induced by the radiolysis of water.[28] Herein, the nitrogen configurations and SSA in NGs have been controlled by changing e-beam irradiation dose. As a result, the low resistance and high SSA of NGs was induced by the proper

[a] Advanced Functional Nanohybrid Material Laboratory, Department of Chemistry, Dongguk University-Seoul, Seoul 100-715, Republic of Korea. E-mail: chemphile@dongguk.edu
[b] Department of Energy and Materials Engineering, Dongguk University-Seoul, Seoul 100-715, Republic of Korea
† Electronic Supplementary Information (ESI) available: See DOI: 10.1039/x0xx00000x

concentration of nitrogen configuration and the generation of micropores depending upon the e-beam irradiation dose. The effects of irradiation dose on the supercapacitor performance of NGs were also evaluated. Thus, the radiolysis method by using e-beam irradiation is a very promising approach to synthesize NGs with the most optimized configurations of doping sites and enhanced SSA for various graphene-based applications.

Experimental section

Preparation of exfoliated GO aqueous dispersion

Aqueous dispersed GO was prepared from commercial graphite (Sigma Aldrich, average size ~20 μm) by using the modified Hummers' method.[29] The as-prepared GO was dispersed in water, following by ultrasonication for 30 min (Sonics, Vibra-Cell, 160 W). After the ultrasonication, the un-exfoliated GO was separated by centrifugation at 3,000 rpm for 10 min to obtain the aqueous dispersion containing well-exfoliated GO nanosheets with the a concentration of ~10.0 mg mL^{-1}.

Synthesis of NGs *via* e-beam irradiation

NGs were synthesized by one-pot radiolysis method using e-beam irradiation in a well-exfoliated GO dispersion in the presence of aqueous ammonia (Daejung, purity 28%). In a typical procedure, a well-exfoliated GO aqueous suspension was diluted by adding a solution of distilled water, isopropyl alcohol as the radical scavenger, and aqueous ammonia as the nitrogen source. The final GO concentration was ~2.0 mg mL^{-1} and the fractions of isopropyl alcohol and aqueous ammonia were ~25% (v/v) and 30% (v/v) in the mixture, respectively. After then, the mixed solution was transferred into an uncovered petri dish and it was placed on the stage equipped with the cooling system for irradiation. For irradiation, e-beam was irradiated at a given amount dose (100, 200, and 300 kGy) with a rectangular beam of 800 mm × 20 mm, at 10 MeV mA^{-1} at room temperature under ambient air conditions. During the irradiation, the stage was moved with a slowly unidirectional reciprocation. The e-beam irradiation was performed at a dose rate of 0.1 kGy s^{-1} in a linear electron beam accelerator (UELV-10-10S) provided by the Advanced Radiation Technology Institute (ARTI) of the Korea Atomic Energy Research Institute (KAERI). Upon e-beam irradiation, the color of the solution immediately turned black from yellow-brown. Finally, the obtained NG suspensions were centrifuged at 8,000 rpm for 10 min and washed several times with ethanol, followed by drying in vacuum oven at 120 °C. Hereafter, the obtained black powders were denoted as NG-dose.

Sample characterization

Structural characteristics of the GO and NGs were obtained by powder X-ray diffractometer (XRD, Rigaku, Ultima IV) equipped with Ni filtered Cu K_α radiation (λ = 1.5418 Å) with a graphite diffracted beam monochromator at a scan rate of 1° min^{-1} from 5° to 50°. The patterns were recorded at an operating voltage and a current of 40 kV and 30 mA, respectively. Raman spectra were obtained using a confocal Raman microscope (Nanobase, Xperam 200) at an excitation wavelength of 532 nm. The morphology of the obtained NG-300 was characterized by field emission scanning electron microscopy (FE-SEM, JEOL, JSM-7100F). For FE-SEM measurements, the powder sample was attached to an Al mount with a carbon tape. X-ray photoelectron spectroscopy (XPS, Thermo Scientific, SIGMA probe) measurements of GO and the NGs using a monochromatized Al K_α X-ray source (1486.71 eV). The sheet resistances of the samples were measured by a four-probe method (Keithley, Model 2000 multimeter). Prior to the XPS and sheet resistance measurement, samples were prepared by pressing the powders into tablets with a diameter of 1 cm under a pressure of 10,000 psi. The chemical compositions were determined by elemental analysis (Thermo Scientific, Flash 2000) with combustion of GO and the NGs powders at 950 °C. To determine the specific surface area and porous properties of the obtained samples, N_2 adsorption-desorption isotherms were measured volumetrically at 77 K (Microtrac, BELsorp-mini II). The GO and NGs were degassed at 80 °C for 12 h and at 120 °C for 5 h, respectively, under vacuum prior to the sorption measurements. The specific surface areas were calculated from the adsorption branch using the Brunauer-Emmett-Teller (BET) method. The pore size distribution was calculated by Barrett-Joyner-Halenda (BJH) method from the nitrogen adsorption isotherm curves.

Electrochemical performance measurements

For the electrochemical performance evaluation of the obtained NGs, the samples were used for electrode active material to fabricate symmetric supercapacitors of coin cell type. In order to prepare electrodes, mixture slurries were prepared by mixing NG powder (80 wt%), polyvinylidene fluoride (PVDF, 15 wt%), and super P (5 wt%) as the conductive agents. Then, these mixture slurries were homogeneously molded in N-methyl-2-pyrrolidone (NMP) and cast on an Al foil current collector by the doctor blade technique at a uniform thickness ~20 μm, and then dried at 120 °C for 5 h in vacuum. Nearly 1.0 mg of active material was loaded at each working electrode. Symmetric supercapacitors were assembled in a CR2032 type coin cell consisting of two electrodes punched into 1-inch diameter and separator. 1 M $LiPF_6$ in a 1:1 mixture of ethylene carbonate and dimethyl carbonate was used as the organic electrolyte. Electrochemical performances were measured based on the galvanostatic charge/discharge curves in the range of 0 – 2.5 V.

Result and discussion

The structural change of GO before and after the e-beam irradiation was investigated by XRD measurement, and the patterns are shown in Fig. 1. The XRD patterns of GO show a sharp diffraction peak of (002) plane at 2ϑ value of 12.9°, but completely disappeared after the e-beam irradiation because

of the removal of oxygen functional groups. Then, a weak and broad diffraction peak in the range ~22.4 – 23.3° of NGs corresponding to the (002) plane of graphite developed, indicating the aggregation of few layer nanosheets and the evolution of graphitic crystal structure.[30] No obvious differences were observed in the broadness of the XRD peaks for samples at various doses, indicating the similar stacking thickness of graphene layers. All the GO and NG samples show the broad (100) diffraction pattern around 42.5°, originating the nature of turbostratic layered structure.[31,32] All NG samples show broader the peak width of (100) diffraction than that of GO, suggesting the graphene-like layers were stacked with a random orientation during the reduction.

Raman analysis is a useful tool to characterize the electronic structure of graphene based materials, particularly for determining ordered and disordered crystal structures of carbon–heteroatoms or carbon–carbon bonds.[33-35] The Raman spectra of graphene-based materials show two featured D and G bands. The G band is induced from the result of the *in-phase* vibration of the E_{2g} mode of the sp^2 carbon domains, whereas the D band is evolved by the disordered crystal structure with symmetry breaking or edges of graphene.[34] The Raman spectrum of the GO and NGs are shown in Fig. 2. After e-beam irradiation, all the G bands of the NGs red-shifted from 1594.5 cm^{-1}, indicating that the sp^2 domains were repaired by e-beam irradiation. As a function of irradiation doses, the G bands of NG-100 and 300 shifted to a lower frequency by ~5.9 cm^{-1}, whereas that of NG-200 moved to a more lower frequency by ~12.7 cm^{-1} with respect to that of GO, indicating that N configurations might be different composition in the obtained NGs. Previously reported theoretical simulations and experimental results on the N configuration effect of NGs indicate that the substitution of carbon atoms with quaternary-N was *n*-type doping, whereas pyridinic-N and pyrrolic-N were *p*-type doping.[12,22,36] The more downshift of the G band in NG-200 compared to other samples, indicate that NG-200 has more *n*-type feature, because of the larger portion of quaternary-N. The shift difference in the NGs corresponded to the previously reported result, which is more downshift in *n*-type than in *p*-type of the NGs.[22,36] Moreover, the reduction of GO or hetero-ion doping significant increased the defect density, along with the increase in the relative intensity ratio between the D and G bands (I_D/I_G). The I_D/I_G was found to increase from 0.88 at GO to ~1.06 – 1.09 at NGs (Table 1), indicating that the NGs have many defects and disorder because of the simultaneous removal of oxygen functional groups and the nitrogen doping.[5]

The FE-SEM images of GO and NG-300 samples show the wrinkled platelet morphology with three-dimensional porous structure, with randomly stacks layer upon layer and are cross-linked (Fig. 3). The morphology of NG-300 is more folded and wrinkled than GO, because of the strong π–π interaction between the reduced GO sheets after e-beam irradiation.[37] The distribution of nitrogen in the sample is highly homogeneous and can be verified using elemental mapping (Fig. S1). The mapping images indicate that the whole basal plane of graphene sheets contains nitrogen atom with a uniform distribution density, evident of a homogenous reaction between GO and NH_3.

The pore structure of the NGs was investigated by N_2 adsorption–desorption analysis. The isotherm curves of NGs as a function of irradiation dose are shown in Fig. 4a. All the adsorption isotherm curves exhibit mixed type I and IV by the IUPAC classification and are indicative of the coexistence of micro- and mesopores in the samples. The hysteresis loop at relative pressures (P/P_0) in the range ~0.4 – 0.6 could be type H2 and H4 hybrid hysteresis by the IUPAC classification, resulting from the combination of slit-like pores between the parallel nanosheets of NGs and interconnected pore system exhibiting constrictions with mesopores.[38] Furthermore, the narrow hysteresis loop indicates that the pores in the obtained samples are quite open.[39] As shown in Table 2, the BET specific surface area (S_{BET}) and total pore volume (V_t) of the obtained NGs significantly increased depending upon the irradiation dose. The S_{BET} of NG-300 was determined to be 470 $m^2\ g^{-1}$ with a total pore volume of 0.273 mL g^{-1}, which is the highest value among the obtained NG series. Indeed, the S_{BET} of samples was less than the theatrical value (>2600 $m^2\ g^{-1}$),[40] because of the shrinking or overlapping of the NG nanosheets by self-aggregation.[36] To evaluate the quantity of micropores in the NGs, *t*-plots were obtained by the calculation from each isotherm curves (Fig. S2), in which the amount of nitrogen adsorbed was plotted against the statistical thickness (*t*) obtained from the standard *t*-curve of graphitized carbon. The micropore diameter gradually decreased from 10.8 to 9.6 Å as a function of the irradiation dose. The micropore volume was evaluated as 0.123 mL g^{-1} for NG-100, and further increased to 0.238 mL g^{-1} with the irradiation time (NG-300). This increment in the micropore volume would be a main factor for generating higher S_{BET}. These results are attributed to the generation of small micropores with the larger amount through the radiation-induced defects at the surface of the NGs, followed by the decrease in the average pore diameter of microproes in the NGs during the irradiation. The pore size distribution curves of the NGs were calculated by the BJH method from the adsorption branch, as shown in Fig. 4b.[41-43] As shown in the figure, the mesopore in a network of the aggregated NGs is estimated to be a broad size distribution of <11 nm.

XPS was further performed to analyze the nitrogen bonding configurations of the NGs depending upon the irradiation dose. The XPS spectra of the GO and NGs over a wide binding energy range of ~100 – 800 eV are shown in Fig. 5a. Two peaks at 284.0 and 532.6 eV can be attributed to the C *1s* and O *1s* signals, respectively.[36] As compared to the GO, the intensity of O *1s* peaks of the NGs significantly decreased and those of the C *1s* peaks increased, indicating that the GO was reduced under e-beam irradiation. In addition, a new N *1s* signal at 399.7 eV was observed for the NG samples, clearly indicating the existence of nitrogen atoms in the NGs. These conclusions were also confirmed by the elemental analysis (Table S1). The fitting of the N *1s* peaks were resolved into four components centered at 398.3, 399.7, 401.2, and 402.5 eV and assigned to pyridinic-N (N-6), pyrrolic-N (N-5), graphitic-N (N-G), and pyridinic-N-oxide (N-X), respectively,[36,39,44] indicating

that nitrogen atoms are in four different configuration sites in the graphene lattice. The results of the deconvolution are shown in Fig. 5b–d and listed in Table 1 for the NG samples. The relative quantities of nitrogen configuration sites were different, and N-5 was the favored form.[5,19,36] This result are similar with the previous report by heating method,[45] suggesting the e-beam is properly new one-pot approach for the synthesis of NGs. The total nitrogen contents and all the N configurations of NG-200 have the highest values among the samples. From the variant of the N configuration portion in the total nitrogen atom, N-G configuration increased and then decreased as a function of irradiation dose, whereas N-5 and N-6 samples showed the reverse tendency (Table S2). In addition, N-X configuration was only presents at NG-200 sample. Thus, we expect that N-G and N-X sites may be induced from N-5 and N-6 during e-beam irradiation.[5] However, when e-beam irradiates at higher dose (above 200 kGy), the increment in the atomic defect of the graphitic lattice was induced by high energy of e-beam, and then the nitrogen contents along with N-G site decreased and N-X site disappeared. We believe that the N-G and N-X sites were easily destroyed under continuous irradiation. The results of this study indicate that the e-beam irradiation method has potential for controlling the N configurations of the NGs by regulating the irradiation dose.

The sheet resistances of the GO and NGs were measured by the four point probe measurement, and the values are listed in Table 1. From these sheet resistances and the thickness of prepared tablet sample, we also can calculate electrical conductivity (Table S3). GO has a high resistance enough to over measurable range, induced from the broken sp^2 conjugated structure by the oxidation reaction, and the decreased sheet resistance is a significant property of the NGs in comparison to GO, reflecting the reduction of GO.[5] NG-200 showed the lowest sheet resistance, because of its high contents of N-G and N-X configurations,[46] whereas the highest sheet resistance of NG-300 can be attributed to its low portion of N-G and N-X configurations and also more defect sites generated by high-energy e-beam irradiation.

As mentioned in the XPS analysis, NGs have four types of N configurations. Among them, N-5 and N-6 have been reported to present *pseudo*-capacitive behavior in aqueous electrolytes, whereas the quaternary N configurations such as N-G and N-X could play an important role in increasing the electrical conductivity and surface charge of NGs.[44] To exclude the *pseudo*-capacitances of N-5 and N-6, the supercapacitor performances were measured in organic electrolytes. Fig. 6a shows the galvanostatic charge/discharge curves of the NGs obtained at a current density of 0.1 A g^{-1}. All the NG samples exhibit much higher specific capacitance than the previously reported value for reduced GO (58 F g^{-1}), indicating that the capacitance improved by nitrogen doping.[5] However, to our surprise, NG-300 sample showed higher specific capacitance of 90.5 F g^{-1} than that of NG-200 (81.8 F g^{-1}), with the highest nitrogen content and quaternary N configuration. This result could be clearly explained by N_2 adsorption–desorption analysis results, where S_{BET} of NGs increased as a function of the irradiation dose. As reported previously, the capacitance of supercapacitor was determined by both the space charge capacitance and electric double layer capacitance. We believe that NG-300 may experience a drastic increase in the electric double layer capacitance, depending on the S_{BET} of sample, although it has the lowest nitrogen contents with quaternary N configuration. Fig. 6b compares the rate performances of the NGs at different current densities. As shown in figure, NG-200 presents the best rate capability of 81.5%, determined by C(10.0 A g^{-1})/C(0.1 A g^{-1}). In addition, the cyclic retentions of NG-100 and 200 samples show more stability without any capacity fade even after 1,000 cycles than that of NG-300 sample, as shown in Fig. 6c. These results indicate that the electrical conductivity is the most important factor for determining the kinetic performance of supercapacitor.

Conclusions

In conclusion, we successfully synthesized NGs by e-beam irradiation in the presence of aqueous ammonia enabling simultaneous reduction of GO and nitrogen doping. The physicochemical analyses indicate that GO was transformed to NGs by the reduction and nitrogen doping. Moreover, the nitrogen configurations and S_{BET} of NGs were controlled by irradiation dose. In the case of supercapacitor application, the increase in the surface area depending upon the irradiation dose attributed NG-300 with the highest capacitance. However, the high quaternary N configuration (N-G and N-X) of NG-200 indicates that the kinetic performance of supercapacitor was enhanced owing to the improvement in the electrical conductivity. Based on our study, this novel doping approach by using e-beam would be a feasible and safe production approach to obtain NGs for various applications.

Acknowledgements

This study was supported by the Basic Science Research Program through the National Research Foundation of Korea (NRF) and the Energy Efficiency and Resources of the Korea Institute of Energy Technology Evaluation and Planning (KETEP) grant funded by the Ministry of Knowledge Economy (No. NRF-2013R1A1A2013035) and the Korean government Ministry of Knowledge Economy (No. 20122010100140).

Notes and references

1 Y. M. Lin, K. A. Jenkins, A. Valdes-Garcia, J. P. Small, D. B. Farmer and P. Avouris, *Nano Lett.*, 2009, **9**, 422-426.
2 M. Pumera, A. Ambrosi, A. Bonanni, E. L. K. Chng and H. L. Poh, *Trac-Trend. Anal. Chem.*, 2010, **29**, 954-965.
3 R. Leary and A. Westwood, *Carbon*, 2011, **49**, 741-772.
4 S. M. Paek, E. Yoo and I. Honma, *Nano Lett.*, 2009, **9**, 72-75.
5 J. Yang, M. R. Jo, M. Kang, Y. S. Huh, H. Jung and Y. M. Kang, *Carbon*, 2014, **73**, 106-113.
6 T. Ramanathan, A. A. Abdala, S. Stankovich, D. A. Dikin, M. Herrera-Alonso, R. D. Piner, D. H. Adamson, H. C. Schniepp, X. Chen, R. S. Ruoff, S. T. Nguyen, I. A. Aksay, R. K.

Prud'homme and L. C. Brinson, *Nat. Nanotechnol.*, 2008, **3**, 327-331.
7 A. K. Geim and K. S. Novoselov, *Nat. Mater.*, 2007, **6**, 183-191.
8 A. H. Castro Neto, F. Guinea, N. M. R. Peres, K. S. Novoselov and A. K. Geim, *Rev. Mod. Phys.*, 2009, **81**, 109-162.
9 C. Lee, X. D. Wei, J. W. Kysar and J. Hone, *Science*, 2008, **321**, 385-388.
10 Y. C. Qiu, X. F. Zhang and S. H. Yang, *Phys. Chem. Chem. Phys.*, 2011, **13**, 12554-12558.
11 P. Nath, S. Chowdhury, D. Sanyal and D. Jana, *Carbon*, 2014, **73**, 275-282.
12 T. Schiros, D. Nordlund, L. Palova, D. Prezzi, L. Y. Zhao, K. S. Kim, U. Wurstbauer, C. Gutierrez, D. Delongchamp, C. Jaye, D. Fischer, H. Ogasawara, L. G. M. Pettersson, D. R. Reichman, P. Kim, M. S. Hybertsen and A. N. Pasupathy, *Nano Lett.*, 2012, **12**, 4025-4031.
13 L. F. Lai, J. R. Potts, D. Zhan, L. Wang, C. K. Poh, C. H. Tang, H. Gong, Z. X. Shen, L. Y. Jianyi and R. S. Ruoff, *Energ Environ. Sci.*, 2012, **5**, 7936-7942.
14 L. P. Zhang and Z. H. Xia, *J. Phys. Chem. C*, 2011, **115**, 11170-11176.
15 A. Lherbier, X. Blase, Y. M. Niquet, F. Triozon and S. Roche, *Phys. Rev. Lett.*, 2008, **101**, 036808.
16 M. Wu, C. Cao and J. Z. Jiang, *Nanotechnology*, 2010, **21**, 505202.
17 D. C. Wei, Y. Q. Liu, Y. Wang, H. L. Zhang, L. P. Huang and G. Yu, *Nano Lett.*, 2009, **9**, 1752-1758.
18 D. Usachov, O. Vilkov, A. Gruneis, D. Haberer, A. Fedorov, V. K. Adamchuk, A. B. Preobrajenski, P. Dudin, A. Barinov, M. Oehzelt, C. Laubschat and D. V. Vyalikh, *Nano Lett.*, 2011, **11**, 5401-5407.
19 H. M. Jeong, J. W. Lee, W. H. Shin, Y. J. Choi, H. J. Shin, J. K. Kang and J. W. Choi, *Nano Lett.*, 2011, **11**, 2472-2477.
20 L. T. Qu, Y. Liu, J. B. Baek and L. M. Dai, *Acs Nano*, 2010, **4**, 1321-1326.
21 X. L. Li, H. L. Wang, J. T. Robinson, H. Sanchez, G. Diankov and H. J. Dai, *J. Am. Chem. Soc.,* 2009, **131**, 15939-15944.
22 D. H. Deng, X. L. Pan, L. A. Yu, Y. Cui, Y. P. Jiang, J. Qi, W. X. Li, Q. A. Fu, X. C. Ma, Q. K. Xue, G. Q. Sun and X. H. Bao, *Chem. Mater.*, 2011, **23**, 1188-1193.
23 C. H. Jung, Y. W. Park, I. T. Hwang, Y. J. Go, S. I. Na, K. Shin, J. S. Lee and J. H. Choi, *J. Phys. D Appl. Phys.*, 2014, **47**, 015105.
24 Y. W. Zhang, H. L. Ma, Q. L. Zhang, J. Peng, J. Q. Li, M. L. Zhai and Z. Z. Yu, *J. Mater. Chem.*, 2012, **22**, 13064-13069.
25 B. W. Zhang, L. F. Li, Z. Q. Wang, S. Y. Xie, Y. J. Zhang, Y. Shen, M. Yu, B. Deng, Q. Huang, C. H. Fan and J. Y. Li, *J. Mater. Chem.*, 2012, **22**, 7775-7781.
26 J. M. Jung, C. H. Jung, M. S. Oh, I. T. Hwang, C. H. Jung, K. Shin, J. Hwang, S. H. Park and J. H. Choi, *Mater. Lett.*, 2014, **126**, 151-153.
27 R. Arrigo, M. Havecker, S. Wrabetz, R. Blume, M. Lerch, J. McGregor, E. P. J. Parrott, J. A. Zeitler, L. F. Gladden, A. Knop-Gericke, R. Schlogl and D. S. Su, *J. Am. Chem. Soc.*, 2010, **132**, 9616-9630.
28 M. Kang, D. H. Lee, Y.-M. Kang and H. Jung, *Electrochimica Acta*, 2015, **184**, 427-435.
29 W. S. Hummers and R. E. Offeman, *J. Am. Chem. Soc.*, 1958, **80**, 1339-1339.
30 I. K. Moon, J. Lee, R. S. Ruoff and H. Lee, *Nat. Commun*, 2010, **1**, 73.
31 U. Hofmann, *Kolloid-Z.*, 1932, **61**, 297-304.
32 H. P. Boehm, *Angew. Chem. Int. Edit.*, 2010, **49**, 9332-9335.
33 A. C. Ferrari, J. C. Meyer, V. Scardaci, C. Casiraghi, M. Lazzeri, F. Mauri, S. Piscanec, D. Jiang, K. S. Novoselov, S. Roth and A. K. Geim, *Phys. Rev. Lett.*, 2006, **97**, 187401.
34 A. C. Ferrari, *Solid State Commun.*, 2007, **143**, 47-57.
35 M. Mowry, D. Palaniuk, C. C. Luhrs and S. Osswald, *Rsc Adv.*, 2013, **3**, 21763-21775.
36 H. L. Guo, P. Su, X. F. Kang and S. K. Ning, *J. Mater. Chem. A*, 2013, **1**, 2248-2255.
37 S. Stankovich, D. A. Dikin, R. D. Piner, K. A. Kohlhaas, A. Kleinhammes, Y. Jia, Y. Wu, S. T. Nguyen and R. S. Ruoff, *Carbon*, **2007**, 45, 1558-1565.
38 J. C. Groen, L. A. A. Peffer and J. Perez-Ramirez, *Micropor. Mesopor. Mat.*, 2003, **60**, 1-17.
39 S. M. Paek, H. Jung, M. Park, J. K. Lee and J. H. Choy, *Chem. Mater.*, 2005, **17**, 3492-3498.
40 H. K. Chae, D. Y. Siberio-Perez, J. Kim, Y. Go, M. Eddaoudi, A. J. Matzger, M. O'Keeffe and O. M. Yaghi, *Nature*, 2004, **427**, 523-527.
41 S. J. Gregg and K. S. W. Sing, *Adsorption, surface area, and porosity*, Academic Press, London ; New York, 2nd edn., 1982.
42 T. Allen, *Particle size measurement*, Chapman and Hall, London ; New York, 4th edn., 1990.
43 E. L. Fuller, *Langmuir*, 2003, **19**, 5052-5057.
44 D. Hulicova-Jurcakova, M. Seredych, G. Q. Lu and T. J. Bandosz, *Adv. Funct. Mater.*, 2009, **19**, 438-447.
45 X. S. Du, C. F. Zhou, H. Y. Liu, Y. W. Mai and G. X. Wang, *J. power sources*, 2013, **241**, 460-466.
46 L. Sun, L. Wang, C. G. Tian, T. X. Tan, Y. Xie, K. Y. Shi, M. T. Li and H. G. Fu, *Rsc Adv.*, **2012**, 2, 4498-4506.

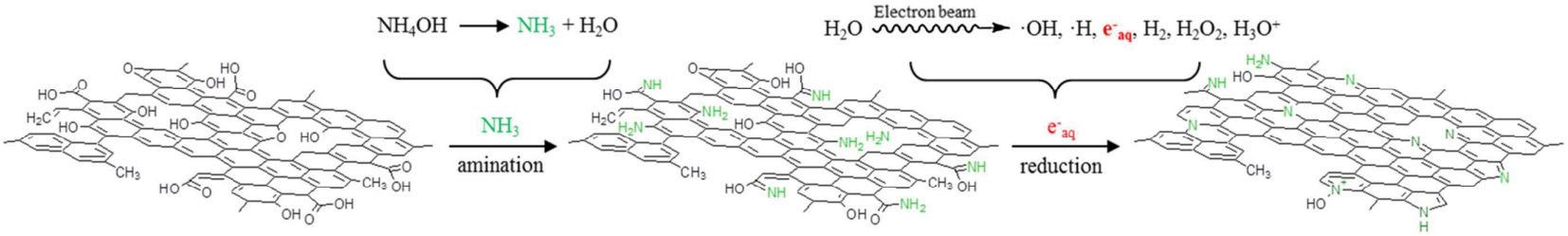

Scheme 1 The schematic representation for the synthesis of NGs by e-beam irradiation.

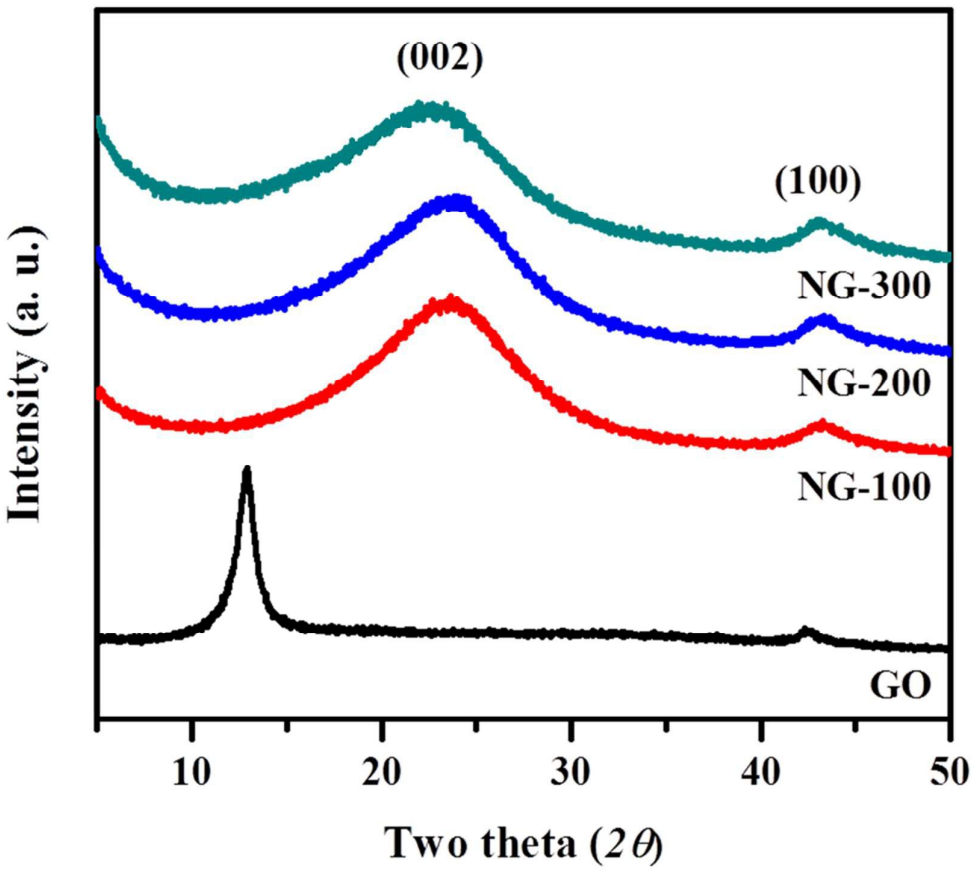

Fig. 1 XRD patterns of the synthesized NGs and GO powder.

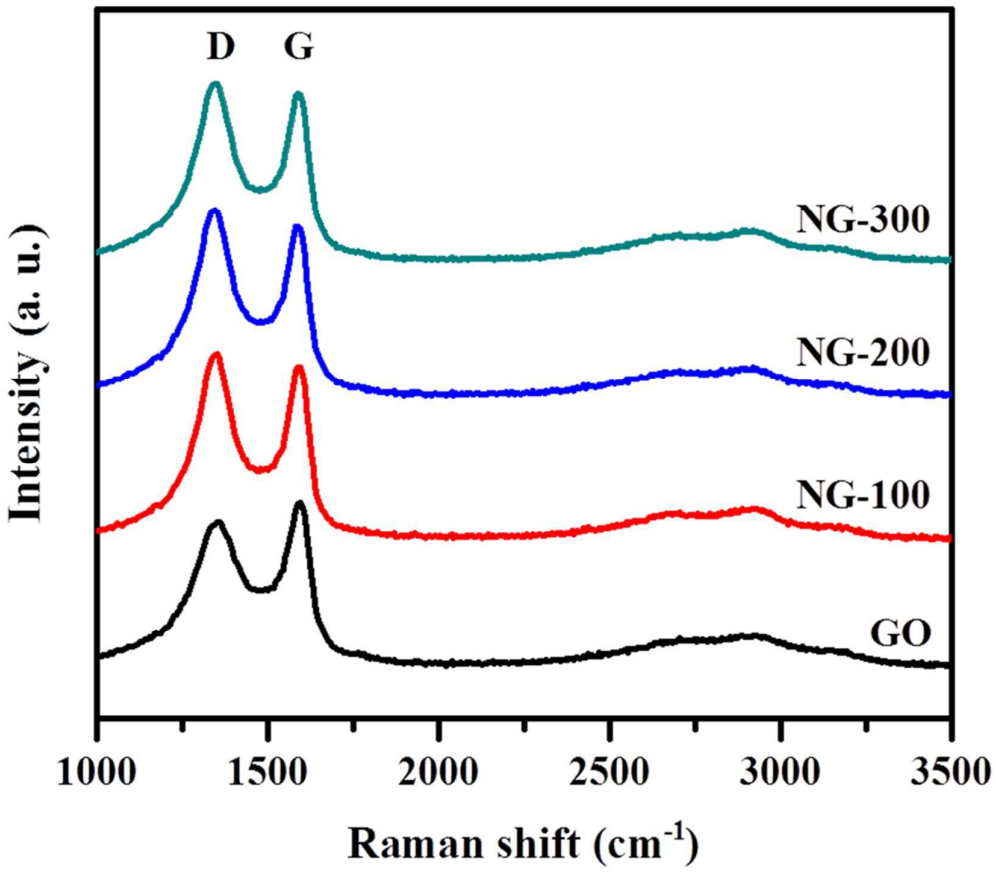

Fig. 2 Raman spectra of GO and NG-100, 200, and 300.

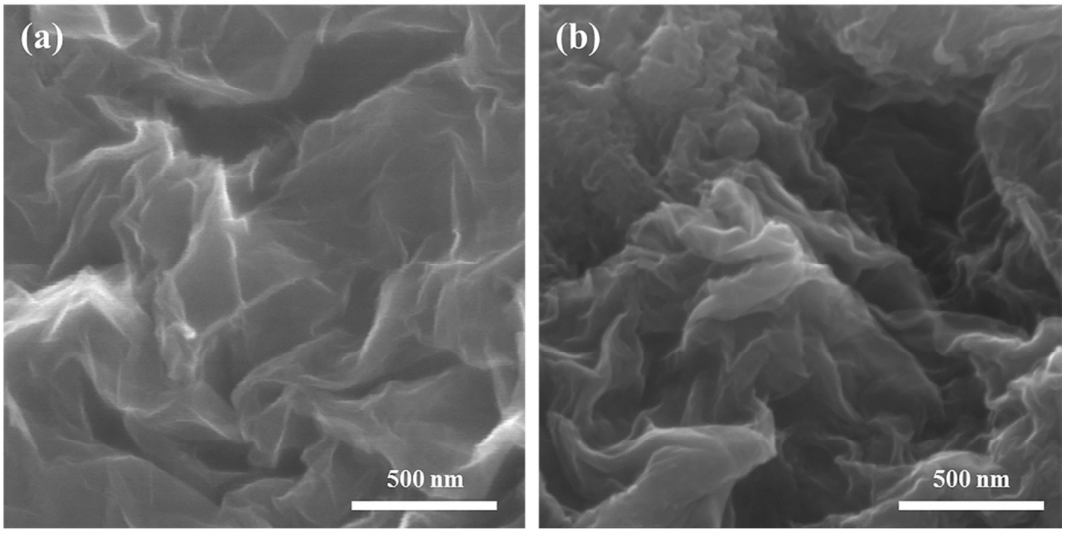

Fig. 3 FE-SEM images of (a) pristine GO, and (b) NG-300.

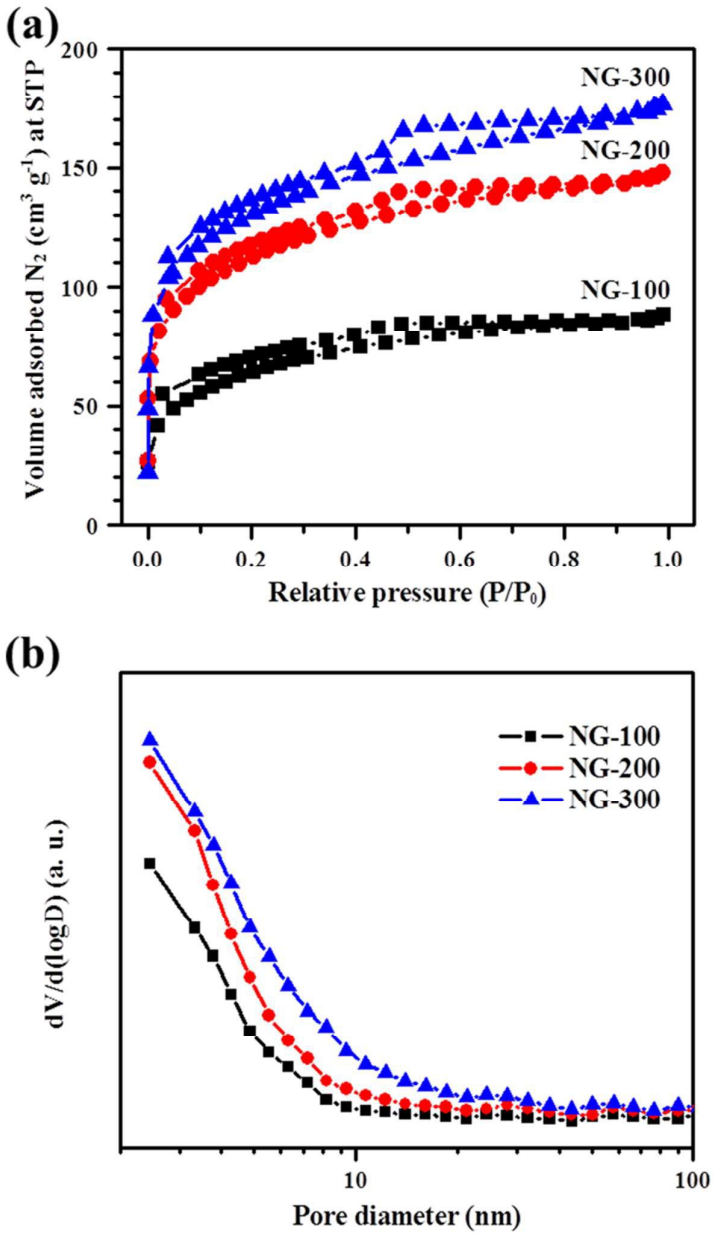

Fig. 4 (a) N_2 adsorption-desorption isotherms and (b) BJH pore size distributions of NG-100, 200, and 300 samples.

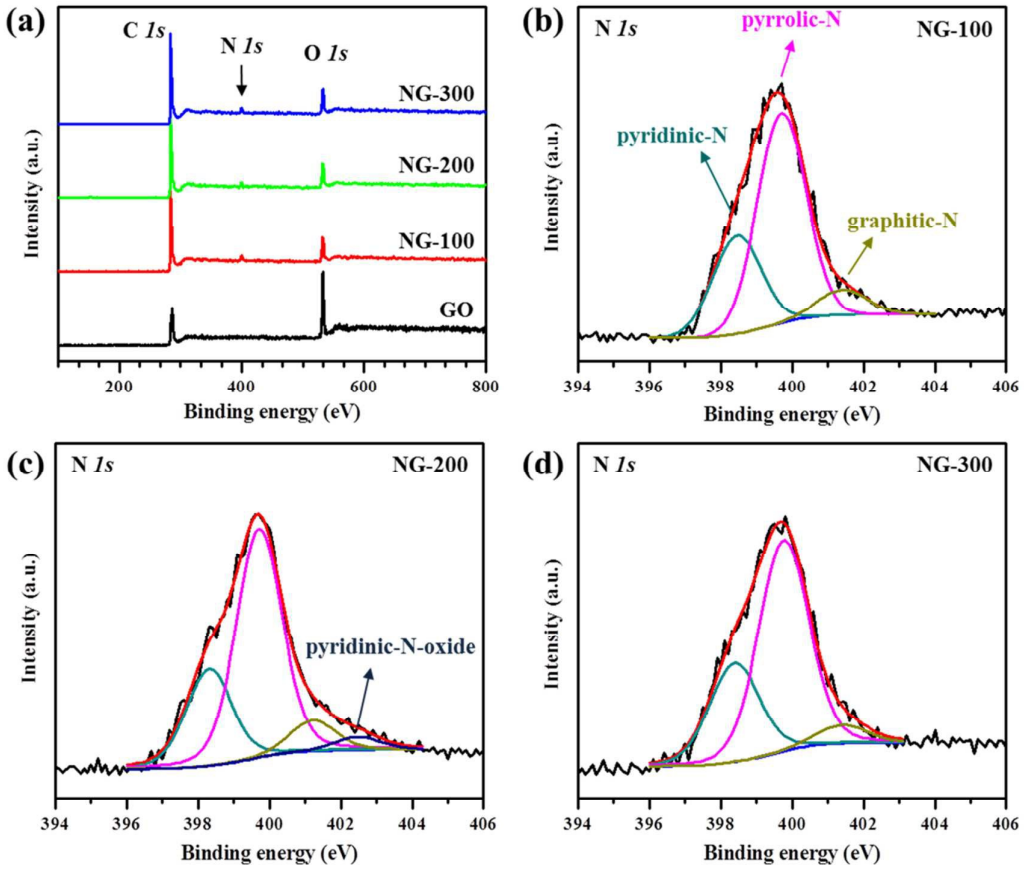

Fig. 5 (a) XPS spectra of GO and NG-100, 200, and 300 samples. Deconvoluted XPS N *1s* spectra of (b) NG-100, (c) NG-200, and (d) NG-300.

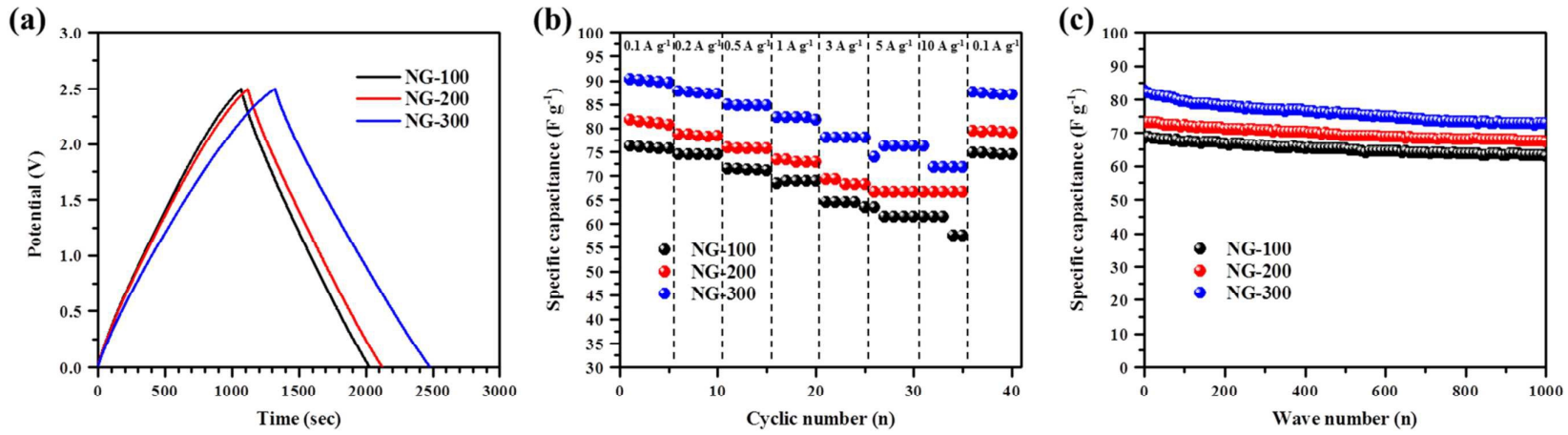

Fig. 6 (a) Galvanostatic charge/discharge curves of NGs. (b) The specific capacitance of NGs at various current densities ranging from 0.1 to 10.0 A g^{-1}. (c) The cyclic retentions of the supercapacitors based on NGs at 1.0 A g^{-1}.

Table 1 Elemental analysis (XPS), sheet resistance, and the ratio of I_D/I_G of the GO and NGs.

Sample	*C (at.%)*[b]	*O (at.%)*[b]	*N (at.%)*[b]	*N-6*[a] *(at.%)*[b]	*N-5*[a] *(at.%)*[b]	*N-G*[a] *(at.%)*[b]	*N-X*[a] *(at.%)*[b]	*Sheet resistance (ohm/sq)*	I_D/I_G
GO	43.67	56.33	-	-	-	-	-	$>10^6$	0.88
NG-100	64.58	31.12	4.29	1.26	2.71	0.32	-	50	1.08
NG-200	64.79	30.25	4.99	1.31	3.10	0.42	0.17	40	1.10
NG-300	66.88	28.82	4.31	1.30	2.78	0.24	-	110	1.06

[a]N-6, N-5, N-G, and N-X are pyridinic-N, pyrrolic-N, graphitic-N and pyridinic-N-oxide, respectively.

[b]The relative contents (at. %) of C, N, O, and N configurations were obtained by the XPS spectra area (C + O + N = 100 at.%, N = N-6 + N-5 + N-G + N-X).

Table 2 BET specific surface area and porous parameters of NGs.

Sample	S_{BET}^{a} ($m^2 g^{-1}$)	V_t^{b} ($ml\ g^{-1}$)	V_{micro}^{c} ($ml\ g^{-1}$)	D_{micro}^{d} (Å)
NG-100	232	0.137	0.123	10.8
NG-200	406	0.229	0.207	9.8
NG-300	470	0.273	0.238	9.6

[a]BET specific surface area calculated from the linear part of the BET plot.

[b]The total pore volume was taken from the volume of nitrogen adsorbed at about $P/P_0 = 0.98$.

[c]The micropore volume was estimated by the *t*-plot.

[d]The average micropore diameter was estimated from by *t*-plot method.

Graphical abstract